Electronic Supplementary Information (ESI)

Structure of lipid multilayers *via* drop casting of aqueous liposome dispersions

*Beatrice Sironi[1], Tim Snow[1], Christian Redeker[1], Anna Slastanova[1], Oier Bikondoa[2,3], Thomas Arnold[4], Jacob Klein[5], and Wuge H. Briscoe[1]**

1. *School of Chemistry, University of Bristol, Cantock's Close, Bristol BS8 1TS, UK*
2. *XMas, The UK-CRG Beamline, The European Synchrotron (ESRF), 71 Avenue des Martyrs, 38043 Grenoble, France*
3. *Department of Physics, University of Warwick, Gibbet Hill Road, Coventry CV4 7AL, UK*
4. *Diamond Light Source, Diamond House, Harwell Science and Innovation Campus, Didcot, Oxfordshire, OX11 0DE, UK*
5. *Material and Interfaces Department, Weizmann Institute of Science, 76100 Rehovot, Israel*

**To whom correspondence should be addressed. Email: wuge.briscoe@bristol.ac.uk*

1. STAI synthesis

Surfactant stearic(C_{18})trimethylammonium iodide, STAI, known also as octadecyltrimethylammonium iodide (formula $CH_3(CH_2)_{17}N^+(CH_3)_3I^-$), was prepared from octadecyltrimethylammonium chloride (STAC) as described in Ref.[1]. Briefly, a potassium iodide aqueous solution (1.39×10^{-3} g L^{-1}) was added to a glass jar containing a basic ion-exchange resin (Dowex 1×8 chloride form, 100-200 mesh). The jar was sealed and put on a roller mixer (Stuart, SRT9D) overnight. The exchange resin was then transferred to a plastic syringe fitted with a cotton pad at the tip of the syringe, and the solution removed by gravity filtration. The resin beads were then rinsed with Milli-Q water (5×20 mL) and transferred in a clean jar. Subsequently, 10 mL of stearoyltrimethilammonium chloride (STAC) aqueous solution (2×10^{-5} g L^{-1}) (Tokyo Chemical Industries, >98%) was added, the jar sealed, and left on the roller for 3 h. A white precipitate of STAI formed. The resin was removed with a sintered funnel and washed with methanol to collect STAI in the filtrate. The solvent was removed *in vacuo* to obtained the raw product, which was finally recrystallized from a methanol:acetone (1:1) mixture three times. The conversion from STAC to STAI was confirmed by elemental analysis (%C: 57.4, %N: 3.3, %I: 28.6, %Cl: 0.0).

2. XRR liquid cell

Referring to Figure 1 in the main text, the liquid cell consists of four stainless steel plates (each 2 mm thick, except for Plate A which is 7.5 mm thick) clamped together, with two 4×4 cm Mylar® windows - one between Plates A and B and the other between Plates C and D,

enclosing the cylindrical sample support to form a sealed chamber of volume ~4-5 mL. Viton O-rings placed between the plates, and between the sample holder and screws ensure sealing of the cell. Inlets and outlets in Plate A allow in situ solution exchange.

3. Synchrotron XRR measurements and sample alignment

XRR measurements were performed at beamline BM28 at the European Synchrotron Radiation Facility (ESRF), Grenoble, France, and also at beamline I07 at the Diamond Light Source (DLS), Didcot, UK. For the measurements, a monochromatic incident X-ray beam irradiated the sample at a grazing angle θ_i (e.g. from 0.06° to 2.6°, corresponding to a Q range of ~0.015 to 0.64 Å-1 for λ = 0.886 Å and to a Q range of ~0.016 to 0.69 Å^{-1} for λ = 0.826 Å, both used at BM28), where the momentum transfer vector normal to the sample's surface is $Q = (4\pi\sin\theta_i)/\lambda$. The specularly reflected intensity was detected at each angle $\theta_r = 2\theta_i$ by an avalanche photodiode detector (APD) for measurements performed at ESRF BM28, and by a Pilatus 100K 2D detector at Diamond Light Source I07. The resulting reflectivity curve can be plotted as reflectivity (a.u.) versus Q (Å^{-1}). The silicon monochromator was tuned to select a given energy E, and the beam size was defined by a set of slits positioned before the sample (BM28) or by a mirror focus (I07). Four different experiments, three at BM28 and one at I07, were performed on DOPC multilayers on bare and PEI-coated mica. The parameters for the three experiments at BM28 were: 1) E = 14 keV (λ = 0.886 Å), beam size = 100 × 280 μm (height (h) × width (w)); 2) E = 14 keV (λ = 0.886 Å), and beam size = 400 × 400 μm ($h \times w$); and 3) E = 15 keV (λ = 0.826 Å), and beam size 800 × 400 μm ($h \times w$); For the Diamond I07 experiment, E = 14 keV and beam size = 60 × 100 μm ($h \times w$). Specular reflections (with $\theta_r = 2\theta_i$) for all samples were collected; for PEI coated mica and STAI coated mica samples, off-specular reflections were also collected, for which the incident and reflection angles were detuned by an off-set of 0.1° at BM28.

At BM28 the liquid cell was mounted on a Huber diffractometer and the sample was aligned with respect to all of the six spatial axes (x, y, z for the three orthogonal translational axes and θ, ϕ, and χ for rotations around these axes, *cf*. Figure 1c in the main text)) so that the beam would be focused to the centre of the sample rotation. At I07 the same liquid cell was used and mounted on a hexapod (PI micros), which allowed independent alignment of the sample with respect to the six spatial axes. Due to the gently curved mica sheet (with the bending axis along the direction of the incident X-ray beam), the sample alignment required careful adjustment of the sample position with respect to all the spatial axes). XRR measurements were typically made at room temperature for all the samples in air, then water was injected into the liquid cell and the measurement repeated, with an integration time of ~1–5 seconds at each angle (e.g. in the range 0.06°–2.6° at BM28) at a typical step size of 0.01°.

4. Contact angle from STAI coated mica

Contact angle of a water droplet on bare mica and STAI-coated mica were measured using a Drop Shape Analyser (DSA100). The angle was determined to be 26° on bare mica and 71° on the STAI-coated mica. The images are shown in Figure S1.

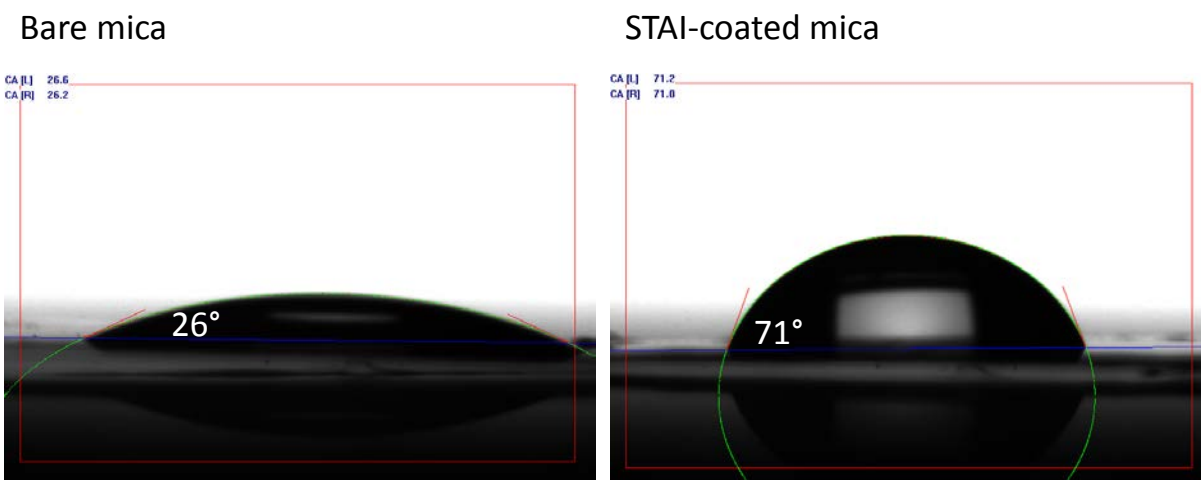

Figure S1: Contact angle measured between water and bare mica, resulting in 26°, and between water and STAI-coated mica, resulting in 71°.

The measured contact angles revealed STAI-coated mica was much less hydrophilic than bare mica. This was expected as STAI adsorbed on the negatively charged mica substrate with its positively charged trimethylammonium headgroup, exposing the hydrophobic tails to the interface, which made increase the contact angle. The contact angle of a DOPC liposome dispersion droplet on these substrates are very similar (images not shown).

5. STAI and PEI coated mica

Coating mica with PEI and STAI polymers results in the presence of a thin film on top of mica, confirmed by the presence of broad Kiessig fringes in the XRR curves for both PEI- and STAI-coated mica (*cf.* Figure S2). In particular, from the Kiessig fringe spacing, the thickness of the PEI layer is estimated to be ~ 25 Å and that of the STAI monolayer ~ 20 Å.

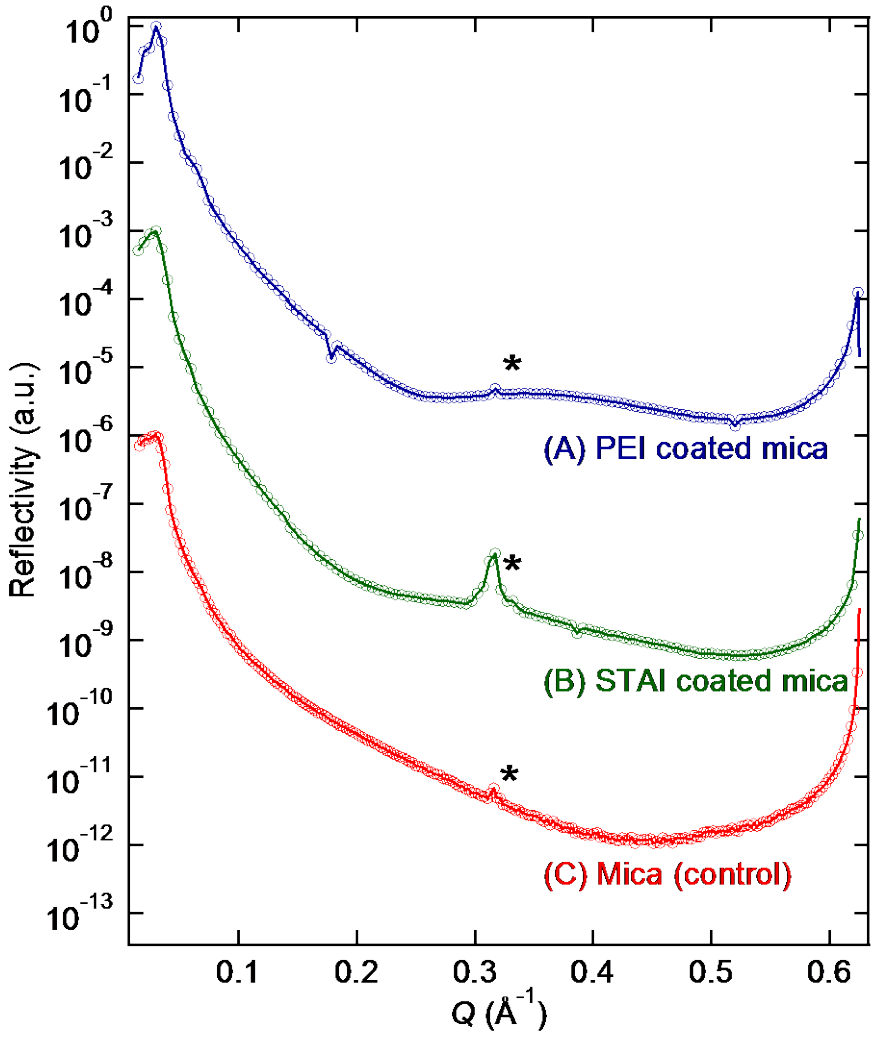

Figure S2: XRR curves for PEI-coated mica, STAI-coated mica and bare mica (as a control) collected in air at room temperature. A mild Kiessig fringe from PEI- and STAI-coated mica reveals the presence of a monolayer film on top of mica surface. The forbidden mica half Bragg Peaks are indicated by (*).

6. Sample alignment in XRR measurements

For the sample alignment, first the height, *z*, was scanned at a $\theta = 2\theta = 0°$ position, with sample raised from below the beam to fully blocking the beam. *z* position was optimized at position where the beam intensity was half of its full intensity (*i.e.* $I_z \sim ½\ I_0$). Then the incident angle θ was raised to $Q \sim 0.63$ Å^{-1} that corresponds to mica's first order Bragg peak angle (*e.g.* at 2.56° for $E = 14$ keV), where the sensitivity is intense and thus suited for alignment, with the detector angle 2θ positioned accordingly to 5.12°. At this position the alignment was optimized for all of the six axes. The alignment was finally checked by performing the rocking curve measurements at four different incident angles (*e.g.* $\theta = 0.1$, 0.2, 0.3, and 0.5°, *i.e.* $Q \sim 0.025$, 0.049, 0.074, and 0.124 Å^{-1} for BM28 measurements at $E = 14$ keV) to confirm that the sample alignment gave maximum reflection intensity at these angles.

7. DOPC multilayer stability in water

Stability of SUV DOPC multilayers in water from a second sample was investigated during another experiment (different from the one presented in the main text). As Figure S3 shows, the multilayer structure was still retained after 2 h. The Scherrer analysis reveals layers of 46.1 Å for the dry sample and of 62.7 Å for the sample under water. Thus the thickness of the dry sample is slightly smaller (by ~ 3 Å) than that of the sample presented in the manuscript, but after hydration the layers swelled to 62.7 Å, which is almost identical to 62.6 Å extracted from Figure 5B (*i.e.* the SUV sample in the main text). XRR curves from MLV sample in air and in water are reported for comparison, which are also presented in Figure 5B.

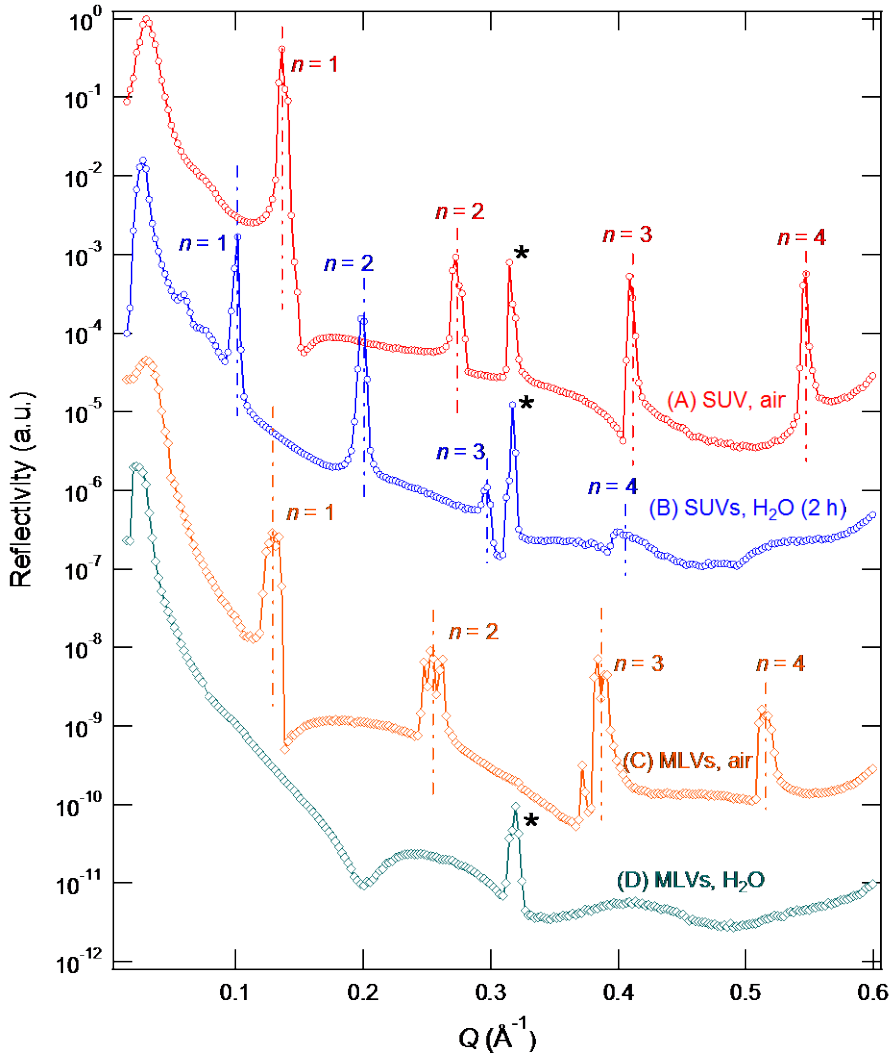

Figure S3: XRR curves for SUV DOPC multilayers on bare mica collected at a different experiment from that shown in Figure 5 of the main text: in air (A), and in water after 2 h (B). For comparison, those for the MLV samples (already shown in Figure 5) are included as (C) and (D). Here the SUV sample was stable against water after 2 h, as indicated by the presence of the Bragg peaks. The mica forbidden half Bragg peaks are marked with an *.

8. DOPC multilayers not reformed after incubation in SUV dispersion

Figure S4 shows XRR curves for the SUV DOPC multilayer sample, to which first water (curve B after 1 h, and curve C after 2 h of exposure to water) and then an SUV DOPC liposome dispersion (lipid concentration ~2 mg L^{-1}; curve D) were added. The multilayer structure was

lost, and only a lipid bilayer remained adsorbed on mica, as indicated by the Kiessig fringes. The drying of the sample after the incubation in the liposome dispersion (Curve E) shows fringes similar to but slightly less pronounced than that of a lipid bilayer under water; however, the absence of Bragg peaks indicates that multilayers did not reform.

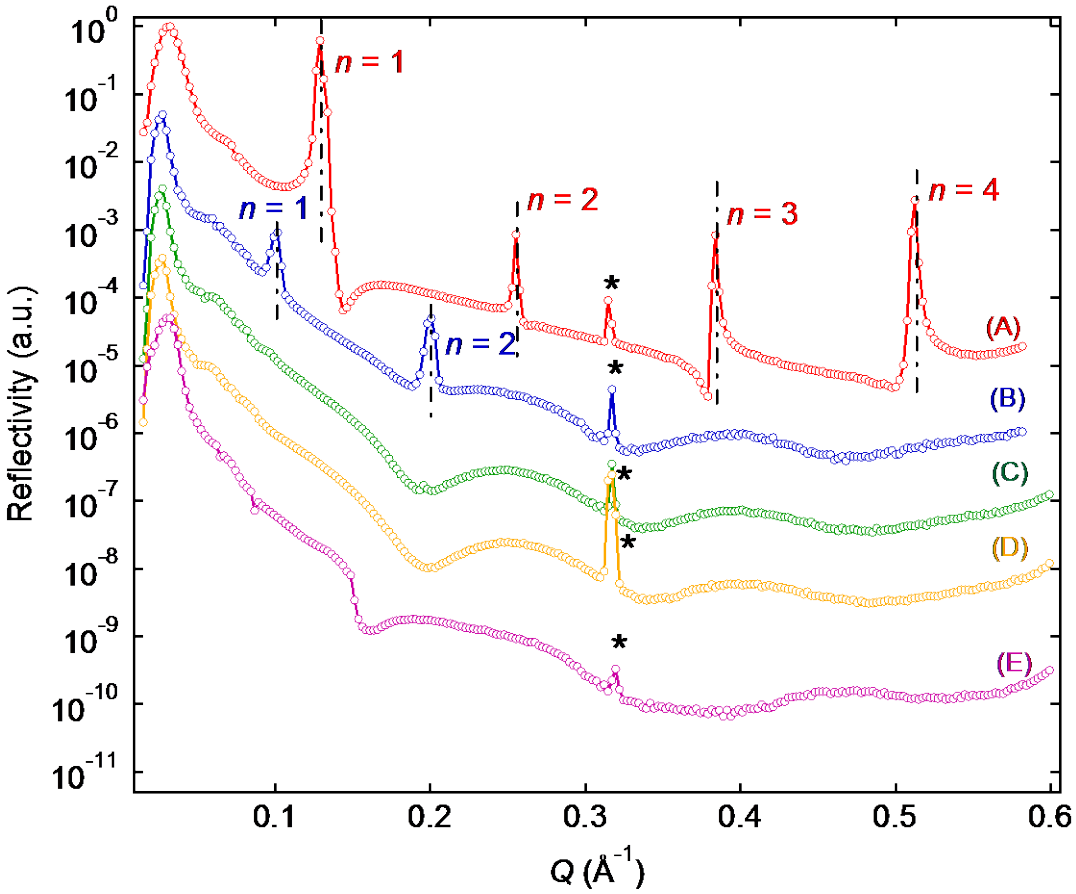

Figure S4: XRR curves for SUV DOPC multilayers on bare mica in air (A), in water after 1 h (B) and 2 h (C), then in an aqueous SUV dispersion for 2.75 h (D), which was then finally dried overnight (E). The mica forbidden half Bragg peaks are marked with an *.

9. Comparison between the XRR curves of the MLV multilayers from BM28 and I07

XRR curves of MLV DOPC multilayers were collected both at BM28 and I07 (*cf.* Figure S5). The two curves belong to two different samples, from two different batches of MLV dispersions, both prepared following the same procedure (as described in the manuscript). The curves show polymorphism in both cases, but the *d* spacing and the coherent length are different. In particular, the curve collected at BM28, discussed in the manuscript, gave the bilayer thickness of ~48.3–49.2 Å, while the sample measured at I07 showed the bilayer thickness ~41.6–46.3 Å. As for the coherent length L_a and the number of layers *m* in the crystalline domains, the BM28 sample exhibited L_a in the range 756–922 Å, corresponding to $m \approx 17–19$. The I07 sample showed pronounced polymorphism, particularly evident from the third order of the Bragg diffraction, resulting in a wide L_a and *m* range (267–968 Å and 6–22 respectively). The differences between the two samples are probably due to the fact that the aggregate size distribution in MLVs was highly polydisperse and not reproducible, resulting in different MLV multilamellar samples. However, the main structural characteristics as

compared to the multilayers prepared from SUVs remain, *i.e.* they exhibited polymorphism and were less well ordered.

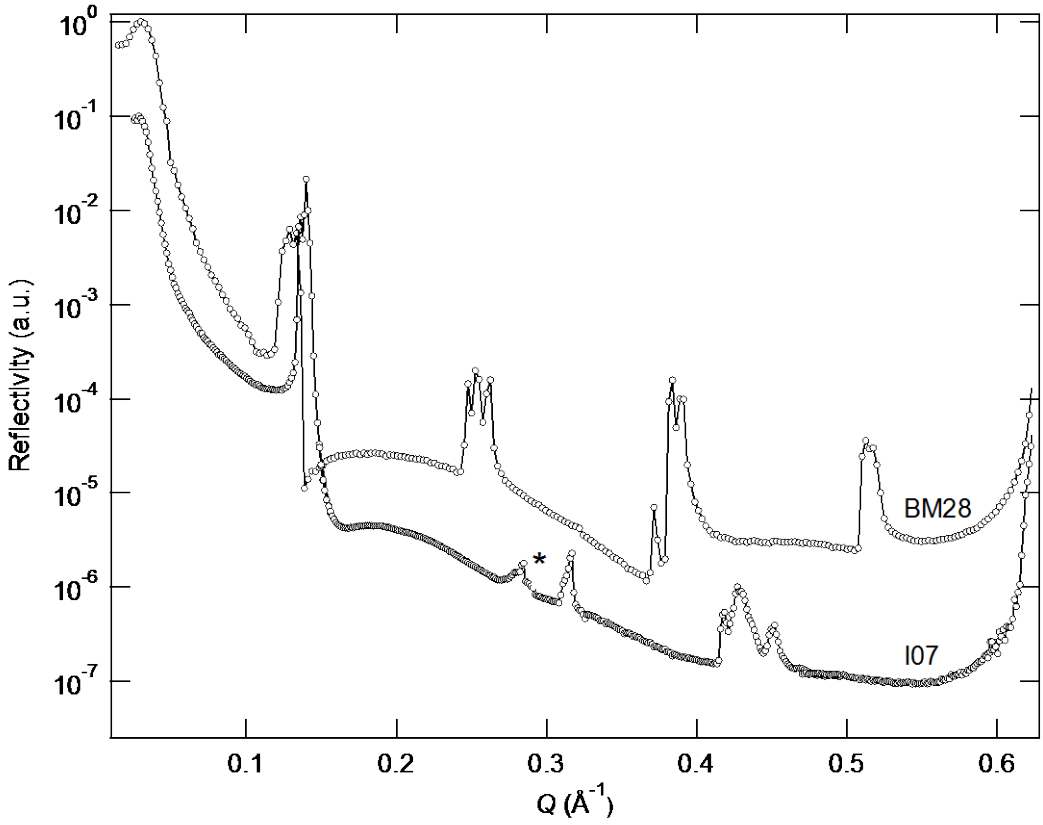

Figure S5: XRR curves for the MLV DOPC multilayers on bare mica in air at room temperature collected from two samples at BM28 (ESRF) and I07 (Diamond Light Source). The mica forbidden half Bragg peak is marked with an *.

10. **Determination of uncertainties**

From the Igor Multipeak fitting package, we have obtained the peak position (Q_n), the width of the peak (*width*), and their uncertainties ($\delta(Q_n)$ and $\delta(width)$ – stored in the Igor waves with the "_Sigma" suffix), and we need to estimate the uncertainties (errors) in the bilayer thickness δd, the coherence length $\delta(L_a)$, and δy for $y = (\Delta Q)^2/(2\pi)^2$ in calculating the paracrystalline disorder.

First, it should be noted that the FWHM (ΔQ) is related to *width* as

$$\Delta Q = 2\sqrt{\ln 2} \cdot width = 1.66511 \cdot width, \quad (1)$$

and thus the uncertainty in the FWHM ($\delta(\Delta Q)$ is

$$\delta(\Delta Q) = 1.66511 \cdot \delta(width). \quad (2)$$

Recall the relevant equations

$$d = \frac{2n\pi}{Q_n} \quad (n = 1, 2, 3, \dots) \tag{3}$$

$$L_a = \frac{2\pi K}{\Delta Q} \quad (where\ K = 1) \tag{4}$$

$$y = \frac{(\Delta Q)^2}{(2\pi)^2} \quad (n = 1, 2, 3, \dots) \tag{5}$$

From these, we obtain

$$\delta d = \frac{2n\pi}{{Q_n}^2}\delta(Q_n)\ (n = 1, 2, 3, \dots) \tag{6}$$

$$\delta(L_a) = \frac{2\pi K}{(\Delta Q)^2}\delta(\Delta Q) \quad (where\ K = 1) \tag{7}$$

$$\delta y = \frac{\Delta Q}{2\pi^2}\delta(\Delta Q) \tag{8}$$

Furthermore, we wish to estimate the uncertainty in the paracrystalline disorder parameter δg from the uncertainty in the slope δm, from the relation

$$g = \frac{1}{\pi}(md^2)^{1/4} \tag{9}$$

Thus,

$$\begin{aligned}\delta g &= \left[\left(\frac{1}{4\pi}d^{\frac{1}{2}}m^{-\frac{3}{4}}\right)^2 (\delta m)^2 + \left(\frac{1}{2\pi}m^{\frac{1}{4}}d^{-\frac{1}{2}}\right)^2 (\delta d)^2\right]^{\frac{1}{2}} \\ &\approx \frac{1}{4\pi}d^{\frac{1}{2}}m^{-\frac{3}{4}}\delta m\end{aligned} \tag{10}$$

Finally, if the intercept of the linear fit to the paracrystalline plot is y_0 and its error from the Igor fit is $\delta(y_0)$, given that the coherence length L_a is

$$L_a = (y_0)^{-1/2}, \tag{11}$$

then

$$\delta(L_a) = \frac{1}{2}(y_0)^{-3/2}\delta(y_0). \tag{12}$$

1. G. Silbert, J. Klein and S. Perkin, Faraday Discussions, 2010, 146, 309-324.